

Article

Comparative Study with ^{89}Y -foil and ^{89}Y -pressed Targets for the Production of ^{89}Zr †

Aiman H. Alnahwi ¹ , Sébastien Tremblay ¹ and Brigitte Guérin ^{1,2,*} 

¹ Department of Nuclear Medicine and Radiobiology, Faculty of Medicine and Health Sciences, Université de Sherbrooke, 12e Avenue Nord, Sherbrooke, QC J1H 5N4, Canada; Aiman.Alnahwi@USherbrooke.ca (A.H.A.); Sebastien.Tremblay@USherbrooke.ca (S.T.)

² Sherbrooke Molecular Imaging Centre (CIMS) of the CRCHUS, 3001, 12e Avenue Nord, Sherbrooke, QC J1H 5N4, Canada

* Correspondence: Brigitte.Guerin2@USherbrooke.ca; Tel.: +1-819-821-8000 (ext. 15285)

† The results have been presented orally at the Society of Nuclear Medicine and Molecular Imaging 2017 Annual Meeting (June 2017, Denver, CO, USA).

Received: 16 August 2018; Accepted: 4 September 2018; Published: 7 September 2018



Abstract: Zirconium-89 (^{89}Zr , $t_{1/2} = 3.27$ days) owns great potential in nuclear medicine, being extensively used in the labelling of antibodies and nanoparticles. ^{89}Zr can be produced by cyclotron via an $^{89}\text{Y}(p,n)^{89}\text{Zr}$ reaction while using an ^{89}Y -foil target. In this study, we investigated for the first time the use of ^{89}Y -pressed target for the preparation of ^{89}Zr -oxalate via a (p,n) reaction. We performed comparative studies with an ^{89}Y -foil target mounted on custom-made target supports. A new automated cassette-based purification module was used to facilitate the purification and the fractionation of ^{89}Zr -oxalate. The effective molar activity (EMA) was calculated for both approaches via titration with deferoxamine (DFO). The radionuclidic purity was determined by gamma-ray spectroscopy and the metal impurities were quantified by ICP-MS on the resulting ^{89}Zr -oxalate solution. The cassette-based purification process leading to fractionation is simple, efficient, and provides very high EMA of ^{89}Zr -oxalate. The total recovered activity was $81 \pm 4\%$ for both approaches. The highest EMA was found at 13.3 MeV and 25 μA for 0.25-mm thick ^{89}Y -foil. Similar and optimal production yields were obtained at 15 MeV and 40 μA while using 0.50-mm thick ^{89}Y -foil and pressed targets. Metallic impurities concentration was below the general limit of 10 ppm for heavy metals in the US and Ph.Eur for both ^{89}Y -foil and pressed targets. Overall, these results show that the irradiation of ^{89}Y -pressed targets is a very effective process, offering an alternative method for ^{89}Zr production.

Keywords: ^{89}Y -pressed target; ^{89}Y -foil; custom-made target supports; proton irradiation; automated cassette-based module; ^{89}Zr -oxalate fractionation; effective molar activity

1. Introduction

Zirconium-89 (^{89}Zr , $t_{1/2} = 78.4$ h) decays via both β^+ emission (22.7%) and electron capture (73.3%) to an intermediate $^{89\text{m}}\text{Y}$ state ($t_{1/2} = 15.7$ s), which decays to stable ^{89}Y via a γ -ray emission of 909 keV. The long half-life of this radionuclide is well suited for the design of radiotracers, such as nanoparticles and monoclonal antibodies (mAb), which require extended in vivo circulation times for optimal biodistribution and tumour targeting [1–3]. ^{89}Zr -based imaging presents numerous advantages, including a sufficiently high abundance of β^+ emission with low maximum energy ($E_{\text{max}}(\beta^+) = 897$ keV and $E_{\text{ave}}(\beta^+) = 396.9$ keV), resulting in a good spatial resolution for mAb-tracking by PET imaging [4–6]. The most widespread application for ^{89}Zr has been the development of immuno-PET tracers based on mAb for in vivo PET cancer imaging. ^{89}Zr -immuno PET can significantly

improve staging, provide an effective method to detect recurrence, and allow for the identification of patients who will be eligible for more personalized and adapted treatment to their specific cancer in order to improve their quality of life.

Zirconium-89 can be produced by cyclotron using three different approaches involving either proton (H^+), deuteron (2H), or alpha (α) particle bombardment [7–11]. The production yield of ^{89}Zr obtained by (p,n) reaction on ^{89}Y is comparable to the one of (p,pxn) reaction on ^{nat}Zr and notably higher than (α ,n) reaction on ^{nat}Sr and (d,2n) reaction on ^{89}Y , along with higher radionuclide purity [9,11,12].

^{89}Y is available under various forms, including foils, wires, and powder with purity greater than 99.6%. The target material is mononuclidic and the use of enriched isotopes for irradiation is unnecessary. ^{89}Y foil is commonly chosen for its availability and easy handling [13,14]. High effective molar activity (EMA) of the isolated ^{89}Zr fractions has been measured while using ^{89}Y -foil [5]. Zirconium-89 can also be produced using a liquid target with yttrium nitrate salts via the $^{89}Y(p,n)^{89}Zr$ reaction. Production of radiometals in solution is challenging due to in-target salt precipitation and unstable target pressures that are caused by gas evolution during irradiation [15]. Moreover, the production yield of ^{89}Zr in solution target is still well below the solid target production yield [5,16]. Zweit et al. showed that the production of no-carrier-added ^{89}Zr from deuteron irradiation of natural ^{89}Y -pressed targets was obtained in high yield, but within the energy window studied, ^{88}Zr was also produced [8]. Other methods, including yttrium-sputtering deposition [17] and spot-welding [18], have been studied for the preparation of ^{89}Zr , but pressing would be advantageous in view of cost and productivity.

In the current study, we investigated for the first time the use of an ^{89}Y pressed powder target to produce ^{89}Zr via proton irradiation. A comparative study with existing ^{89}Y -foil target is presented in order to outline the full potential of this novel pressed target. We studied the dimension and thickness of the solid targets under different irradiation conditions and we optimized the design of the target supports. We also developed an automated extraction and purification process while using a cassette-based module allowing for the fractionation of ^{89}Zr . Results are presented and discussed with the objective of maximizing the thickness of the solid targets and obtaining high-yield, high-purity, and high-EMA as ^{89}Zr -oxalate.

2. Materials and Methods

2.1. Materials

All the chemicals and solvents were purchased with high purity and were used as is unless otherwise specified. Yttrium-89 foil (0.127 and 0.25-mm thick, 99.9%) and yttrium-89 powder 40-mesh (99.6%) with different metal composition (Table 1) were bought from Alfa Aesar (Ward Hill, MA, USA/VWR International, CA).

Table 1. Trace metal analysis for ^{89}Y -foil and powder (Certificate of analysis).

Metal (ppm) ¹	Fe	Al	Mn	Ca	Cu	Gd	Mg	Nd	Zr	Mo
^{89}Y -foil ²	<110	<100	<100	<100	<100	<100	<100	<100	np	np
^{89}Y -powder ³	~2000	45	46	~2000	55	100	540	200	2.8	4.7

¹ Not all elements are mentioned in this table. Fe: Iron, Al: Aluminum, Mn: Manganese, Ca: Calcium, Cu: Copper, Gd: Gadolinium, Mg: Magnesium, Nd: Neodymium, Zr: Zirconium, and Mo: Molybdenum. ² Y-Foil (99.9%).

³ Y-Powder (Alfa Aesar, 99.6%). Not present (np).

Hydrochloric acid (99.999%), oxalic acid (99.999%), Na_2CO_3 (99.999%) trace metal basis, sodium hydroxide pellets ($\geq 98.0\%$), diethylenetriaminepentaacetic acid (DTPA, $\geq 99\%$), and deferoxamine (DFO) mesylate salt ($\geq 92.5\%$) were purchased from Sigma-Aldrich (Saint-Louis, MO, USA). High-purity water (Optima LC/MS, ultra-high performance liquid chromatography ultraviolet grade, 0.03-mm filtered) and acetonitrile (HPLC grade, 99.9%) were purchased from Fisher Scientific

(Ottawa, ON, CA). All the glass vials were cleaned while using chromic sulfuric acid (Fisher Scientific, Ottawa, ON, CA). Instant thin layer chromatography-silica gel (ITLC-SG) was acquired from Agilent Technology (Santa Clara, CA, USA). The labeling efficiency of ^{89}Zr -DFO was determined while using radio-ITLC-SG with 100 mM DTPA as the mobile phase. The radio-ITLC plates were scanned using an instant imager scanner (Bioscan, DC, USA). Radioactivity measurements were performed in an ionization chamber (CRC-25PET; Capintec) on the ^{89}Zr setting to control process efficiency and by γ -ray spectrometry with a calibrated high-purity germanium detector (GMX HPGe; ORTEC, Oak Ridge, TN, USA) for analytic quantitation. Experimental samples were counted for 10 min by using dynamic energy windows of 1–2000 keV. All of the radioactive detection devices were calibrated and maintained in accordance with our routine quality control procedures.

2.2. Cyclotron Targetry and Irradiation

Irradiations were performed using TR19 and TR24 variable energy (H^- : 13–19 and 16.2–24 MeV, respectively) cyclotrons (ACSI, Richmond, BC, Canada) while using a straight 90° target station (ACSI). ^{89}Zr was produced via the $^{89}\text{Y}(p,n)^{89}\text{Zr}$ transmutation reaction while using a solid ^{89}Y -foil or pressed target mounted on custom-made aluminum and niobium coin target supports (Figure 1). Irradiation times (T_{irr}) were 1–5 h with a beam current of 10–40 μA for both cyclotrons. The beam size in all irradiation experiments was ~ 10 mm in diameter. The incident proton-beam energies were selected based on the degrader materials used and varied between 16.2–18 MeV. The proton-beam energies deposited on the target materials were 11.3–15 MeV for all the productions and they were calculated by Monte Carlo simulation while using SRIM [19]. The ACSI small solid target irradiation station provided efficient target cooling through a helium gas jet directed on the front side of the target while the backside was cooled by chilled water (16.5–18.5 $^\circ\text{C}$).

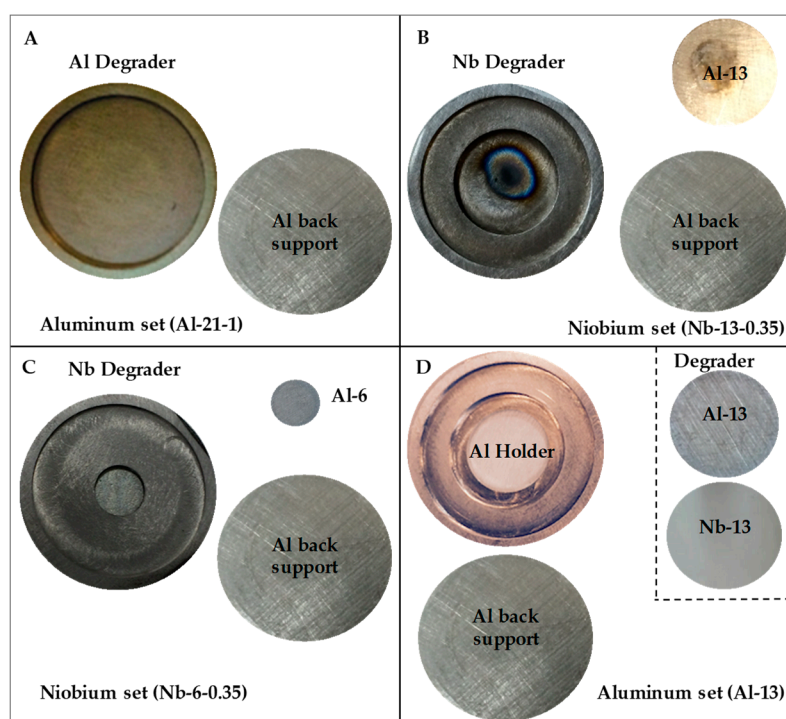


Figure 1. Photographs of the CIMS' (Sherbrooke Molecular Imaging Centre) custom-made degraders and holder for the $^{89}\text{Y}(p,n)^{89}\text{Zr}$ reaction. (A) Al degrader with a thickness of 1.0 mm and a hole diameter of 21 mm (Al-21-1). (B) Nb degrader with a thickness of 0.35 mm and a hole diameter of 13 mm (Nb-13-0.35). (C) Nb degrader with a thickness of 0.35 mm and a hole diameter of 6 mm (Nb-6-0.35). (D) Al open window target holder with an inner diameter of 13 mm (Al-13).

2.3. Solid Target Design and Preparation

Four aluminum and niobium coin target holders/degraders were custom-designed and manufactured at the Department of Physics's machine shop of the Université de Sherbrooke (Figure 1). Both aluminum and niobium coins have an outer diameter of 24 mm and a thickness of 2 mm to fit in the small solid target station, which can accommodate no more than 2.2-mm thick targets. Initially, the first target body Al-21-1, presenting a hole diameter of 21 mm and a thickness of 1 mm, was made from 6061-T6 aluminum alloy to accommodate a thickness of 0.254 mm of ^{89}Y -foil at maximum (Figure 1A). As the proton beam size of both cyclotrons is ~ 10 mm, the hole diameter of the niobium degraders was reduced to 13 mm (Nb-13-0.35) and 6 mm (Nb-6-0.35) to accommodate a 1-mm thick ^{89}Y -foil/pressed powder (Figure 1B,C). An aluminum open window holder with a hole diameter of 13 mm (Al-13) was also designed to be used with a degrader (Figure 1D). As shown in Figure 1B–D, small aluminum disks (13 and 6 mm diameter) were used when needed to fill the gap between ^{89}Y -pressed or foil targets and the aluminum back support for improvement of targets cooling during the irradiation. The aluminum back supports were machined with a thickness of 0.5 mm for Al-13 holders when compared to a thickness of 1.0 mm for all other degraders. Target assembly was performed without applying pressure on target material, foil, or pellet. The procedure to assemble the targets is illustrated in Figure S1 of the Supplementary Information.

Before pressing, inert gas (N_2) was applied into the hole in the die. The ^{89}Y powder was inserted and pressed into either 6 or 13 mm diameter pellets ranging in thickness from 0.3 to 0.5 mm. The maximum pressure applied to 6 and 13 mm dies was 3500 and 18,000 pounds per square inch, respectively, while using a digital hydraulic carver press (Module number: 3912, Carver, Inc, Wabash, IN, US). The pellets were placed in the target holders and covered with a degrader. ^{89}Y -foil targets of various thicknesses ranging from 0.25 to 0.51 mm were mounted on the custom-made holders (Figure S1). Niobium and aluminum degraders were installed on the He/beam side to avoid problems, while mounting and dismounting the disc set in the cyclotron solid target station. For the optimization of the production yield, seven 0.89-mm thick ^{89}Y foils were mounted together in a round shaped 6-mm diameter Nb-6-0.35 degrader.

2.4. Automated Cassette-Based Module and Separation Chemistry for ^{89}Zr -oxalate

A cassette-based purification module obtained from ACSI was modified in-house to remotely produce ^{89}Zr -oxalate inside a hot-cell. The front panel of the module was equipped with two cassettes, one to allow for easy load of the liquid vials, the other for dispensing of three vials (Figure 2 and Figure S2).

The glass dissolution vial was prewashed with concentrated 6N trace metal HCl for at least 24 h. Prior to perform purification, three and five manifold kits were installed and the unit was cleaned using 6N trace metal HCl. To avoid solvent leaks, all the liquids were transferred through the system by polytetrafluoroethylene (PTFE) tubing while using a negative pressure generated by a peristaltic pump with a flow rate of 4 mL/min. To reduce exposure to metal that can affect EMA, all the liquid and gas connections were assembled while using PTFE and silicon connectors. Before each production, all solutions (30 mL of 2N trace metal HCl, 20 mL of high-purity water, and 3 mL of 1 M oxalic acid) were preloaded into the module. Hydroxamate resin (100 mg) prepared and functionalized following the procedure reported by Holland et al. was packed in a 1 mL cartridge between two frits (20 microns) (United chemical technologies, Bristol, PA, USA) [5]. The hydroxamate column was preconditioned with 8 mL of acetonitrile, 20 mL of high-purity water, and 3 mL of 2N trace metal HCl. The module was controlled by a laptop computer and the module functions by an easy to program user interface (RSView 32 software, Rockwell Software, Milwaukee, WI, USA).

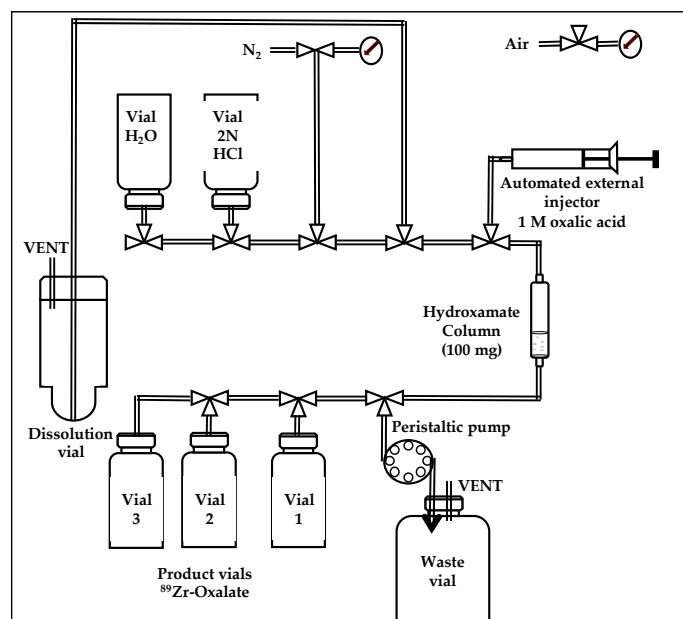


Figure 2. Schematic diagram of the ^{89}Zr oxalate purification panel.

After irradiation and decay of the short half-life $^{89\text{m}}\text{Zr}$ ($t_{1/2} = 4.16$ min), either $^{89}\text{Y}/^{89}\text{Zr}$ foil, or pressed target was removed from the degrader/holder and was directly dropped in the dissolution vial and then dissolved with 10 mL of 2N trace metal HCl for 3–5 min at room temperature. If the foil and pressed targets overheated, they required more time for a complete dissolution in HCl. The crude solution was then loaded and passed through the hydroxamate resin in the cartridge and transferred to the waste using a negative pressure created by the peristaltic pump. The column was washed with 2N trace metal HCl (20 mL) and high-purity water (20 mL). Then, a low helium pressure (20 psi) was applied to dry the line and the cartridge. Finally, the Zr-89 bound to the column was eluted with 0.5 mL of 1M oxalic acid under helium pressure (20 psi). This process was repeated twice to collect three 0.5-mL fractions in different vials. EMA was determined for each fraction. The fourth fraction was collected for half-life measurement.

2.5. Effective Molar Activity Using DFO Chelator

EMA (GBq/ μmol) of ^{89}Zr was calculated via titration with DFO and the purified combined ^{89}Zr -oxalate fractions 1 and 2. Solutions of DFO (0.5 mL in 1.5-mL microcentrifuge tube) at different concentrations (380.6 to 2.3×10^{-5} nmol) were prepared via serial dilution. After 1 h incubation time with ^{89}Zr (0.9 to 1.1 MBq, 50 μL), the solutions of DFO were quenched while using DTPA (40 μL , 1 mmol) for 10 min to complex free ^{89}Zr . After incubation and quenching with DTPA, the EMA was determined by measuring the DFO labelling efficiency with ITLC-SG analysis using DTPA (100 mM) as a mobile phase solvent. ^{89}Zr -DTPA complex eluted with the solvent front, whilst ^{89}Zr -DFO complex remained at the origin. ITLC-SG was analyzed using Radio-ITLC scanner. The binding percentages were plotted on a sigmoidal dose-response curve. EC_{50} value, which is reflecting the molar concentration at 50%, was calculated by prism 7 software (GraphPad Software Inc, La Jolla, CA, USA). The EMA was calculated as two times the EC_{50} value.

2.6. Determination of Radionuclide and Metal Impurities

Samples containing 148–222 kBq of purified fraction of ^{89}Zr -oxalate in a 1.5 mL microcentrifuge tube were diluted with high-purity water to bring a final volume of 0.5 mL. The radionuclidic purity was determined by γ -ray spectroscopy on a HPGe detector with zoom energy window of 1–2000 KeV. With that amount of radioactivity, the dead time was below 5%. Samples were counted for only 10 min after the end of synthesis. In addition, the test was repeated after six months to qualify radionuclide

impurities with long half-life, such as ^{88}Y ($t_{1/2} = 106.6$ d) and ^{88}Zr ($t_{1/2} = 83.4$ d); they were not present in the formulated ^{89}Zr . The half-life was estimated using dose calibrator CRC-55 PET and was calibrated at 465. Trace metal analysis in ^{89}Zr -oxalate solutions that were produced while using ^{89}Y -foil and ^{89}Y -pressed powder as starting materials was performed by inductively coupled plasma mass spectroscopy (ICP-MS) for 31 metals in compliance with USP <233> (Exova, St-Augustin-de-Desmaures, QC, Canada).

3. Results

3.1. Cyclotron Production Yield and Degraders Used

Several experiments were performed while using ^{89}Y -foil and pressed-powder with the different target holders and degraders in aluminum and niobium designed for the ^{89}Zr production on TR24 and TR19 cyclotrons (Figure 1). Pressing procedures were optimized to provide reproducible and consistent density pellets. Yttrium powder from Alfa Aesar formed successfully compact pressed targets. The preparation and assembly of ^{89}Y -pressed target are very fast and can be done in few minutes.

Targets characteristics, measured production yields, and EMA are summarized in Table 2. The proton energies deposited on the targets were maintained between 11–15 MeV for most of our irradiations. The irradiations were first performed on ^{89}Y -foil target. The production yield using Al-21-1 degrader was 26.4 MBq/ $\mu\text{A}\cdot\text{h}$ using ^{89}Y -foil (Table 2, entry 1). A similar production yield was obtained by using Nb-13-0.35 degrader and about half the quantity of target material (entry 2). We noticed damage (overheating) to the Nb-13-0.35 degrader when the irradiation time was increased to 4.2 h with a beam current of 10 μA (Figure 1B).

The ^{89}Zr yield was well correlated with proton energy (E_p) and target thickness. By keeping constant the amount of target material and the foil thickness, a slightly higher yield of 27.8 MBq/ $\mu\text{A}\cdot\text{h}$ was obtained by increasing the proton-beam energy deposited to the target material from 11.3 to 13.3 MeV (entries 2–3). When the Y-foil thickness was doubled while using two stacked 0.25-mm thick foils, the production yield was improved to 36.6 MBq/ $\mu\text{A}\cdot\text{h}$ (entries 3 and 6). The amount of ^{89}Zr produced increased proportionally by increasing the current from 15 to 25 μA with similar production yields (entries 3–5). Similar production yields were also obtained for irradiations that were made on TR19 and TR24 by selecting the appropriate degrader thickness (entries 3–4).

To establish the optimal target thickness for the production of ^{89}Zr , a stacked foil technique was used. The proton-beam energy deposited to the target material was fixed at 11.3 MeV (Figure 3). Similar production yields were found for the first four foils of 6 mm diameter facing the proton beam, indicating that the optimal target thickness was ~ 0.50 mm. Using these conditions, the production yield was 17.1 MBq/ $\mu\text{A}\cdot\text{h}$.

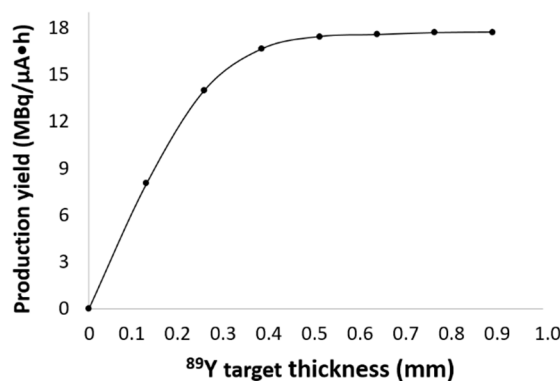


Figure 3. Optimization of production yield using foil targets.

Table 2. Targets characteristics, measured production yields and effective molar activity (EMA).

Entry	Target	Mass (mg)	⁸⁹ Y-Thickness (mm)	Beam Degradar Material/Thickness		E _p (MeV) ¹	T _{irr} (h)	Current (μA)	Yield (MBq/μA·h)	EMA (GBq/μmol)
1	foil	273	0.25	Al	1.00 mm	11.3 ²	3.0	15.3	26.4	85
2	foil	145	0.25	Nb	0.35 mm	11.3 ³	3.0	10.0	24.3	59
3	foil	142	0.25	Al	0.48 mm	13.3 ⁴	4.8	15.4	27.8	172
4	foil	152	0.25	Al	0.29 mm	13.3 ⁴	4.7	20.2	27.3	288
5	foil	155 ± 4	0.25	Al	0.29 mm	13.3 ⁴	4.8	25.1	26.9 ± 1.4	329 ± 69
6	foil	312	0.50	Nb	0.35 mm	13.3 ³	4.2	9.9	36.6	51
7	foil	303	0.50	Al	0.48 mm	15.0 ⁴	1.5	40.3	54.0 ± 2.9	129 ± 7
8	pressed	141 ± 5	0.35	Nb	0.35 mm	11.3 ³	3.0	10.0	22.7 ± 1.2	39 ± 10
9	pressed	157	0.30	Al	0.29 mm	13.3 ⁴	4.9	23.9	20.7 ± 1.2	156 ± 32
10	pressed	247	0.51	Nb	0.13 mm	13.3 ⁴	4.2	15.1	37.2 ± 1.3	88 ± 23
11	pressed	247	0.50	Al	0.48 mm	15.0 ⁴	1.5	42.3	49.5 ± 1.2	117 ± 13

¹ Proton-beam energies were calculated by Monte Carlo simulation using SRIM. ² Al-21-1 degrader was used. ³ Nb-13-0.35 degrader was used. ⁴ Al-13 holder was used. TR19 cyclotron was used for experiments reported in entries 4, 5, 9, and 10 only.

The highest production yield of 56.1 MBq/ $\mu\text{A}\cdot\text{h}$ was found by increasing the proton-beam energy deposited on the target material up to 15.0 MeV while using an 0.5-mm foil thickness and the Al-13 holder (Table 2, entry 7). Moreover, a current of 40 μA can be applied on the target without any target overheating when using an Al-13 holder for the irradiation (entries 7 and 11).

The irradiations were initiated on a 0.35-mm thick ^{89}Y -pressed target. When the 13-mm diameter pressed target was used with Nb-13-0.35 degrader, the production yield was 22.7 ± 1.2 MBq/ $\mu\text{A}\cdot\text{h}$ for a proton-beam energy that was deposited on the target material of 11.3 MeV (entry 8). As seen before for ^{89}Y -foil targets, the production yield increased by almost two-fold, reaching 37.2 ± 1.3 MBq/ $\mu\text{A}\cdot\text{h}$, when increasing the target thickness from 0.30 to 0.51 mm and using similar irradiation conditions (entries 9 and 10). A high production yield of 49.5 ± 1.2 MBq/ $\mu\text{A}\cdot\text{h}$ was also obtained for ^{89}Y -pressed target at the optimum ~ 0.5 mm thickness and E_p of 15.0 MeV at 40 μA (entry 11). Using these irradiation parameters, similar and optimal production yields were obtained for both ^{89}Y -foil and pressed targets (entries 7 and 11).

3.2. Automated Cassette-Based Module, Separation Chemistry

The ^{89}Zr was processed by an automated cassette-based module designed by ACSI for radiometal purification (Figure 2 and Figure S2). The user interface software allows for the operator to control the module for producing and purifying ^{89}Zr -oxalate from irradiated ^{89}Y -foil and pressed targets. Among the ~ 50 productions performed, only two productions failed due to cracked or leaking reused manifolds. Before ^{89}Zr elution, large volumes of 2N trace metal HCl and high-purity water were used to remove Fe^{3+} and other metals present in ^{89}Y -powder and foil. Typically, the recovered activity was $81.0 \pm 4.4\%$ when combining fractions 1–4 and the maximum activity was found in the second product fraction formulated in 0.5 mL of 1M of oxalic acid. Minimal losses occurred, with some ^{89}Zr being recovered in the dissolution vial ($3.8 \pm 1.2\%$), in waste ($0.5 \pm 0.3\%$), or trapped on the resin ($5.0 \pm 2.8\%$), the 3M manifold ($1.5 \pm 1.1\%$), or the 5M manifold ($0.1 \pm 0.1\%$) (Figure 4). The entire procedure, from dissolution to collection of ^{89}Zr fractions, takes less than 30–35 min. After dissolution, $\sim 95\%$ of the activity is transferred to hydroxamate resin and more than 80% of initial activity is collected in a total of 2 mL (4×0.5 mL) oxalic acid (fractions 1–4).

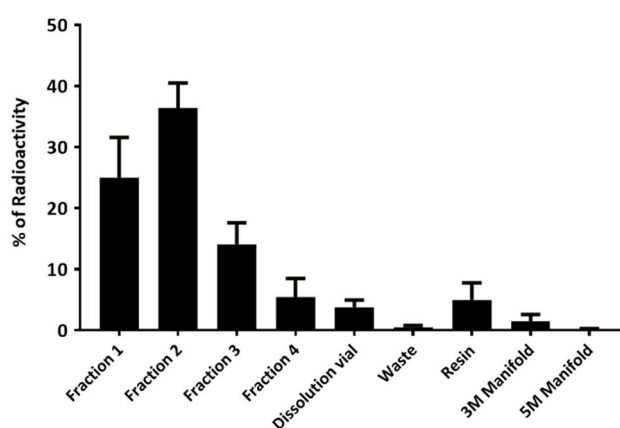


Figure 4. Recovered and residual ^{89}Zr activities in the purification module components ($n = 7$).

3.3. Effective Molar Activity and Radionuclide and Metals Impurities

The EMA of the isolated ^{89}Zr -oxalate was experimentally determined by the DFO titration method and the purified combined fractions 1–2. In all isolated purified solution, the EMA of ^{89}Zr -oxalate for foil and pressed targets were found to be in the range of 51–329 GBq/ μmol and 39–156 GBq/ μmol , respectively (Table 2). It was noticed that EMA increased proportionally with increasing irradiation time (Table 2, entries 2 and 3), beam current, and the proton-beam energy deposited on the target (entries 2 to 5) to reach 329 ± 69 GBq/ μmol (8892 ± 1865 Ci/mmol) for the ^{89}Y -foil target, the highest EMA

value reported at this time to our knowledge. However, EMA decreased when increasing the target thickness and the amount of ^{89}Y irradiated (entries 5 and 6). The EMA values were, to some extent, almost similar at 15 MeV and 40 μA while using 0.50-mm thick ^{89}Y -foil and pressed targets (Table 2, entries 7 and 11). In addition, it was noticed that EMA of the isolated ^{89}Zr -oxalate and recovery activity were higher in purified fractions 1 and 2 for both ^{89}Y -pressed target and ^{89}Y -foil (Table 3).

Table 3. EMA values and activities for ^{89}Y -pressed target and ^{89}Y -foil.

Fraction (0.5 mL)	^{89}Y -pressed Target		^{89}Y -foil	
	EMA ¹ (GBq/ μmol)	Recovered Activity (MBq)	EMA ¹ (GBq/ μmol)	Recovered Activity (MBq)
1	150 \pm 34	754 \pm 3	278 \pm 115	1013 \pm 258
2	162 \pm 30	1232 \pm 100	379 \pm 23	1081 \pm 175
3	43 \pm 25	109 \pm 62	157 \pm 95	368 \pm 125

¹ Irradiation was performed for 5 h on 0.3-mm thick ^{89}Y -target using the Al-13 holder, 0.3-mm thick Al degrader and a proton-beam energy of 13.3 MeV.

To estimate the radionuclidic purity of ^{89}Zr after purification, γ -ray spectroscopy was performed. Using ^{89}Y -foil as starting material, two peaks with high intensities at 511 and 911 keV were observed (Figure 5A). In addition, measurements were repeated after six months to allow for a complete decay of ^{89}Zr . Spectra of γ -ray showed no presence of ^{88}Zr (393 keV) and ^{88}Y (898 and 1836 keV) impurities [20] (Figure 5B) when the irradiation was done at 11.3 MeV. However, three peaks corresponding to ^{88}Zr (<0.001%) and ^{88}Y impurities were clearly observed on the γ -ray spectrum six-month post-purification of ^{89}Zr irradiated at 13.3 MeV (Figure 5C). As obtained with purified ^{89}Zr from ^{89}Y -foil, no impurities of ^{88}Zr and ^{88}Y were noted at six-month post-purification for ^{89}Zr that was produced at 11.3 MeV from ^{89}Y -pressed powder. Nevertheless, small intensity peaks corresponding to long half-life radiometals, such as Co-57 (122 keV, $t_{1/2} = 271.79$ d), Co-58 (511 keV, $t_{1/2} = 70.86$ d), and Co-56 (846 and 1238 keV, $t_{1/2} = 77.7$ d), were observed at this time point (Figure 5D). They probably originated from iron impurities in ^{89}Y -pressed powder (Table 1) via $^{58}\text{Fe}(p,n)^{58}\text{Co}$, $^{56}\text{Fe}(p,n)^{56}\text{Co}$, $^{57}\text{Fe}(p,n)^{57}\text{Co}$, and $^{58}\text{Fe}(p,2n)^{57}\text{Co}$ reactions. In addition, the 1460 keV peak decayed from K-40 ($t_{1/2} = 1.28 \times 10^9$ y, 0.0117% neutral abundance) [21–23].

The metal impurities were quantified by ICP-MS for ^{89}Zr -oxalate fraction 2 samples that were produced by cyclotron, while using ^{89}Y -foil or pressed powder as starting materials (Table 4 and Table S1). Metallic impurities were below the general limit of 10 ppm for heavy metals in the US and Ph.Eur for both ^{89}Y -foil and pressed targets. Impurity metal concentrations, such as antimony, arsenic, barium, beryllium, bismuth, cadmium, chromium, cobalt, copper, lithium, magnesium, manganese, molybdenum, nickel, selenium, silver, strontium, thallium, tin, titanium, vanadium, and lead, were below the detection limit of <1.0 ppm in all analyzed samples.

Table 4. Inductively coupled plasma mass spectroscopy (ICP-MS) analysis of the decayed ^{89}Zr -Oxalate fraction 2 samples from ^{89}Y -Foil and ^{89}Y -pressed powder ($n = 2$).

Metal (ppm) *	Y	Fe	Al	Mn	Ca	Cu	Mg	Zn	Mo
^{89}Zr -Oxalate ¹	<0.08	<4.17	<1.8	<0.1	<7.4	<1.0	<3.2	<5.2	<1.0
^{89}Zr -Oxalate ²	<0.44	<4.17	<0.8	<0.1	<3.0	<1.0	<1.0	<4.6	<1.0

¹ From ^{89}Y -foil target. ² From ^{89}Y -pressed target. * Volume was 0.5 mL for each decayed sample. 31 element values are listed in Table S1.

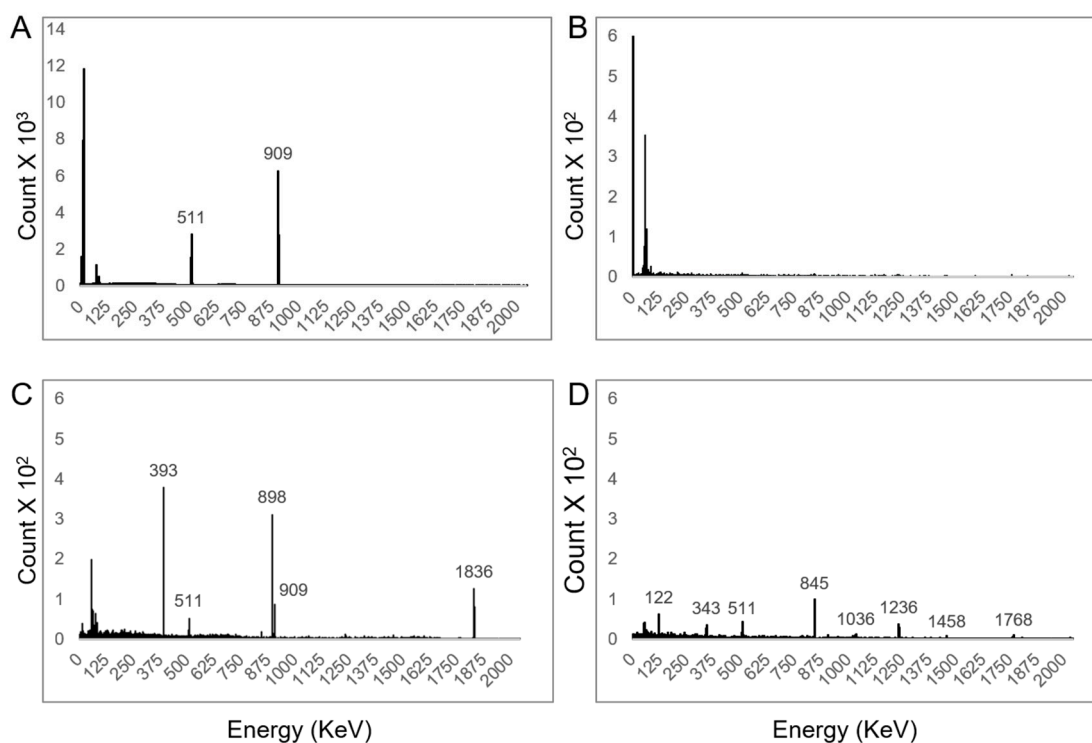


Figure 5. Representative γ -spectra of ^{89}Zr performed after (A) ^{89}Zr purification using ^{89}Y -foil and irradiation performed at 11.3 MeV, (B) six months, using ^{89}Y -foil and irradiation performed at 11.3 MeV, (C) six months, using ^{89}Y -foil and irradiation performed at 13.3 MeV, and (D) six months, using ^{89}Y -pressed powder and irradiation performed at 11.3 MeV. Samples were measured using a HPGe detector.

4. Discussion

According to data reported by Mustafa et al., the optimal cross-section is at 750.8 ± 1.5 mb while using 12.46 MeV E_p [7]. Increasing E_p beyond this level will increase the ^{89}Zr production yield, but long half-life by-products, such as ^{88}Zr and ^{88}Y , will then be produced. Thus, ^{89}Zr production is not optimal using medium energy cyclotron, except considering the reduction of the E_p , which can be achieved with an energy degrader. We designed different size target degraders and holders in different materials (Figure 1) to be used with incident E_p of 16.2–18 MeV. An aluminum holder/degrader was first selected for its high-energy transfer [13], which renders more efficient target cooling during the irradiation. Niobium has high chemical resistance and was selected due to its high melting temperature and to avoid any deterioration of the target body during cleaning with hydrochloric acid to remove any trace of unknown metals [14].

The degradation of the beam energy with our designed degraders was achieved without damage, except for the Nb degrader while using long irradiation times (Figure 1B). Under these conditions, the ^{89}Y -pressed powder oxidized into Y_2O_3 , which is poorly soluble and required a high volume of 12N HCl for its dissolution and purification [24]. Furthermore, the aluminum degrader presents better heat transfer and no local overheating was observed for the Al-21-1 degrader (Figure 1A) when 15 and 40 μA were applied to ^{89}Y -foil at 13.3 and 15 MeV for 4.5 and 1.5 h, respectively.

The production yield depends on the incident E_p , the degrader material, and the beam size, as well as the density and thickness of the target materials. The highest yields were found for 0.50-mm thick ^{89}Y -foil target (two foils). Increasing the number of foils beyond this thickness did not improve the yield for an E_p of 11.3 MeV. The production yield was also affected by the target diameter. Indeed, higher yields were obtained with the 13-mm diameter targets that provided a better fit with the beam size of ~ 10 mm. One should note that a current as high as 40 μA could be applied when the Al-13

holder was used as compared to all other degraders, the cooling system being more efficient. Indeed, the Al back support is thinner for the Al-13 holder (0.5 mm) as compared to that of other degraders (1.0 mm) (Figure 1). In addition, high production yield values were obtained while using both foil and pressed targets.

The highest yield (54 ± 2.9 MBq/ $\mu\text{A}\cdot\text{h}$) obtained at 15.0 MeV is similar to that the one reported by Holland et al. (56.24 ± 4.1 MBq/ $\mu\text{A}\cdot\text{h}$) [5] for a similar foil target thickness. As shown in Table 2, the production yield reported for ^{89}Y -pressed target (49.5 ± 1.2 MBq/ $\mu\text{A}\cdot\text{h}$) is slightly lower than the one that was reported by Zweit et al. (66.6 MBq/ $\mu\text{A}\cdot\text{h}$) while using ^{89}Y -oxide pressed targets irradiated at 16.2 MeV from deuteron [8]. Zweit et al. reported that the increase of beam current and irradiation time was more challenging using pressed targets [8]. In the present study, we were able to irradiate at 15 and 40 μA for 4.2 and 1.5 h, respectively, without overheating the ^{89}Y -target material.

The automated cassette-based module that was used in this work is simple, reliable, and provides reproducible results with high-recovered activity. The system can accommodate three separate product vials with independent controlled valves that gives an advantage over the automated purification box developed by Wooten et al. that eluted purified ^{89}Zr in only one fraction vial [14]. As the maximum activity and EMA were found in fractions 1 and 2 (Figure 4 and Table 3), we usually prefer to combine only these two fractions for further studies. Using our system, greater EMA (1378 to 8892 vs. 5 to 353 Ci/mmol), more efficient separation with higher ^{89}Zr recovered activity ($81 \pm 4.4\%$ vs. $74 \pm 16\%$) and lower ^{89}Zr retention on the column ($5 \pm 2.8\%$ vs. $18 \pm 15\%$) were obtained, when compared to Wooten's results [14].

Commonly, to achieve high EMA, the chemical must be metal trace with high purity ^{89}Y . To our knowledge, we reported in these studies the highest EMA values for ^{89}Zr that were produced by cyclotron by optimizing the E_p , the amount/thickness and the current applied on the ^{89}Y -target. The highest EMA values were obtained while using packed ^{89}Y -foils. The EMA values achieved while using ^{89}Y -pressed targets well improves the value reported by Holland et al. [5]. Pressed ^{89}Y targets are easy to prepare compared to electro-deposition preparation methods, which are also time consuming and less expensive compared to ^{89}Y -foil. They could represent an excellent alternative for routine production of ^{89}Zr . The preparation of both foil and pressed targets can be done in a few minutes. The cost for ^{89}Y -foil is ~ 108 US\$/irradiation using 2 foils (0.5-mm thickness and 13-mm diameter), while for ^{89}Y powder (0.5-mm thickness, 13-mm diameter, and 250 mg), the cost is ~ 3 US\$/irradiation, without considering the equipment costs. Admittedly, the use of pressed target comes at the cost of purchasing a press. This alternative strategy can rapidly be cost-effective if the press is used in the development of other solid targets and/or if the price of ^{89}Y -foil rises.

One should note that ^{89}Y -powder 40-mesh (99.6% purity) that was used in this work contains more impurities than ^{89}Y -foil (99.9% purity). Particularly, 2000 ppm of Fe^{+3} in ^{89}Y powder is responsible for the presence of the low amount of long half-life radiometal impurities ($^{56,57,58}\text{Co}$) observed six months post irradiation. However, the metal impurity contents were almost similar for purified ^{89}Zr -oxalate solutions obtained from ^{89}Y -foil and pressed targets and it did not affect the labelling of ^{89}Zr with deferoxamine chelator (Table 4).

Using our irradiation parameters and 11.3 MeV E_p for production of ^{89}Zr , no radionuclide impurities, such as ^{88}Zr and ^{88}Y were observed in purified fractions. However, when we increased the E_p to 13.3 MeV, trace of ^{88}Zr and ^{88}Y were observed on γ -ray spectrum measured after six months in the residual ^{89}Zr product solution after decay. The presence of ^{88}Y in the product solution after ^{89}Zr decay is not associated with the poor separation efficiency of the hydroxamate column, but is related to the decay chain of ^{88}Zr to ^{88}Y . E_p increases the production yield as well as the EMA, but it also increases production of long half-life impurities. This contamination will not affect image quality nor increase significantly the radiation exposure of the patient, but it must be considered when managing radioactive waste.

5. Conclusions

In this work, we successfully design solid target degraders/holders for ^{89}Zr production while using foil and pressed targets. The cassette-based purification process that is described in this work is both simple and efficient and can be used for routine ^{89}Zr production. Degrading the proton energy to 15 MeV provides high yields of ^{89}Zr , sufficient for (pre)clinical use and/or commercial supply. ^{89}Y -pressed target holds great potential and offers an alternative method for the production of ^{89}Zr . EMA of purified ^{89}Zr fractions were found to be superior to the reported values and appropriate for antibody-based PET Imaging.

Supplementary Materials: The following are available online at <http://www.mdpi.com/2076-3417/8/9/1579/s1>, Figure S1: Solid target assembly, Figure S2: Remote-controlled automated cassette-based module for ^{89}Zr -oxalate. Table S1: Elements analyzed by ICP-MS for ^{89}Zr -oxalate produced by cyclotron using ^{89}Y -foil and pressed targets.

Author Contributions: Conceptualization, B.G. and S.T.; Methodology, A.H.A.; Validation, S.T.; Formal Analysis, A.H.A., S.T. and B.G.; Writing-Original Draft Preparation, A.H.A.; Writing-Review & Editing, S.T. and B.G.; Supervision, S.T. and B.G.; Project Administration, B.G.; Funding Acquisition, B.G.

Funding: The present study was financially supported by the Natural Sciences and Engineering Research Council of Canada (NSERC, RGPIN-2014-04354).

Acknowledgments: Brigitte Guérin is a member of the CRCHUS (CIUSSS de l'Estrie-CHUS) funded by the Fonds de recherche du Québec-Santé (FRQS) and holder of the Jeanne and J.-Louis Lévesque Chair in Radiobiology at Université de Sherbrooke. The present study was financially supported by the Natural Sciences and Engineering Research Council of Canada [NSERC, grant no. RGPIN-2014-04354]. Aiman H. Alnahwi received a scholarship from the King Fahad Specialist Hospital-Dammam, Kingdom of Saudi Arabia. We gratefully acknowledge Jean-François Beaudoin and the Department of Physics of the Université de Sherbrooke for their assistance in the design and the preparation of the target degraders/holder. We thank cyclotron operators Eric Berthelette, Paul Thibault and Luc Parenteau for providing excellent help with the irradiations.

Conflicts of Interest: The authors declare no conflict of interest.

References

1. Meijs, W.E.; Haisma, H.J.; Van Der Schors, R.; Wijbrandts, R.; Van Den Oever, K.D.; Klok, R.P.; Pinedo, H.M.; Herscheid, J.D.M. A facile method for the labeling of proteins with zirconium isotopes. *Nucl. Med. Biol.* **1996**, *23*, 439–448. [[CrossRef](#)]
2. Meijs, W.E.; Haisma, H.J.; Klok, R.P.; van Gog, F.B.; Kievit, E.; Pinedo, H.M.; Herscheid, J.D. Zirconium-labeled monoclonal antibodies and their distribution in tumor-bearing nude mice. *J. Nucl. Med.* **1997**, *38*, 112–118. [[PubMed](#)]
3. Boerjesson, P.K.E.; Jauw, Y.W.S.; de Bree, R.; Roos, J.C.; Castelijns, J.A.; Leemans, C.R.; van Dongen, G.A.M.S.; Boellaard, R. Radiation dosimetry of Zr-89-labeled chimeric monoclonal antibody U36 as used for immuno-PET in head and neck cancer patients. *J. Nucl. Med.* **2009**, *50*, 1828–1836. [[CrossRef](#)] [[PubMed](#)]
4. Laforest, R.; Liu, X. Image quality with non-standard nuclides in PET. *Q. J. Nucl. Med. Mol. Imaging* **2008**, *52*, 151–158. [[PubMed](#)]
5. Holland, J.P.; Sheh, Y.; Lewis, J.S. Standardized methods for the production of high specific-activity zirconium-89. *Nucl. Med. Biol.* **2009**, *36*, 729–739. [[CrossRef](#)] [[PubMed](#)]
6. Zhang, Y.; Hong, H.; Cai, W. PET tracers based on Zirconium-89. *Curr. Radiopharm.* **2011**, *4*, 131–139. [[CrossRef](#)] [[PubMed](#)]
7. Mustafa, M.G.; West, H.I.; O'Brien, J.H.; Lanier, R.G.; Benhamou, M.; Tamura, T. Measurements and a direct-reaction-plus-Hauser-Feshbach analysis of the $^{89}\text{Y}(p,n)^{89}\text{Zr}$, $^{89}\text{Y}(p,2n)^{88}\text{Zr}$, and $^{89}\text{Y}(p,pn)^{88}\text{Y}$ reactions up to 40 MeV. *Phys. Rev.* **1988**, *38*, 1624–1637.
8. Zweit, J.; Downey, S.; Sharma, H.L. Production of no-carrier-added zirconium-89 for positron emission tomography. *Int. J. Radiat. Appl. Instrum. Part A* **1991**, *42*, 199–201. [[CrossRef](#)]
9. Uddin, M.; Baba, M.; Hagiwara, M.; Tarkanyi, F.; Ditroi, F. Experimental determination of deuteron induced activation cross sections of yttrium. *Radiochim. Acta* **2007**, *95*, 187–192. [[CrossRef](#)]
10. Kandil, S.A.; Spahn, I.; Scholten, B.; Saleh, Z.A.; Saad, S.M.M.; Coenen, H.H.; Qaim, S.M. Excitation functions of (α, xn) reactions on ^{nat}Rb and ^{nat}Sr from threshold up to 26 MeV: Possibility of production of ^{87}Y , ^{88}Y and ^{89}Zr . *Appl. Radiat. Isot.* **2007**, *65*, 561–568. [[CrossRef](#)] [[PubMed](#)]

11. Ivanov, P.I.; Jerome, S.M.; Bozhikov, G.A.; Maslov, O.D.; Starodub, G.Y.; Dmitriev, S.N. Cyclotron production and radiochemical purification of $^{88,89}\text{Zr}$ via α -particle induced reactions on natural strontium. *Appl. Radiat. Isot.* **2014**, *90*, 261–264. [[CrossRef](#)] [[PubMed](#)]
12. Uddin, M.S.; Khandaker, M.U.; Kim, K.S.; Lee, Y.S.; Lee, M.W.; Kim, G.N. Excitation functions of the proton induced nuclear reactions on natural zirconium. *Nucl. Instrum. Methods Phys. Res. Sect. B Beam Interact. Mater. Atoms* **2008**, *266*, 13–20. [[CrossRef](#)]
13. Lin, M.; Mukhopadhyay, U.; Waligorski, G.J.; Balatoni, J.A.; Gonzalez-Lepera, C. Semi-automated production of ^{89}Zr -oxalate/ ^{89}Zr -chloride and the potential of ^{89}Zr -chloride in radiopharmaceutical compounding. *Appl. Radiat. Isot.* **2016**, *107*, 317–322. [[CrossRef](#)] [[PubMed](#)]
14. Lake Wooten, A.; Madrid, E.; Schweitzer, G.D.; Lawrence, L.A.; Mebrahtu, E.; Lewis, B.C.; Lapi, S.E. Routine production of ^{89}Zr using an automated module. *Appl. Sci.* **2013**, *3*, 593–613. [[CrossRef](#)]
15. Pandey, M.K.; Engelbrecht, H.P.; Byrne, J.P.; Packard, A.B.; DeGrado, T.R. Production of ^{89}Zr via the $^{89}\text{Y}(p,n)^{89}\text{Zr}$ reaction in aqueous solution: Effect of solution composition on in-target chemistry. *Nucl. Med. Biol.* **2014**, *41*, 309–316. [[CrossRef](#)] [[PubMed](#)]
16. Pandey, M.K.; Bansal, A.; Engelbrecht, H.P.; Byrne, J.F.; Packard, A.B.; DeGrado, T.R. Improved production and processing of ^{89}Zr using a solution target. *Nucl. Med. Biol.* **2016**, *43*, 97–100. [[CrossRef](#)] [[PubMed](#)]
17. Queern, S.L.; Aweda, T.A.; Massicano, A.V.F.; Clanton, N.A.; El Sayed, R.; Sader, J.A.; Zyuzin, A.; Lapi, S.E. Production of Zr-89 using sputtered yttrium coin targets ^{89}Zr using sputtered yttrium coin targets. *Nucl. Med. Biol.* **2017**, *50*, 11–16. [[CrossRef](#)] [[PubMed](#)]
18. Ellison, P.A.; Valdovinos, H.F.; Graves, S.A.; Barnhart, T.E.; Nickles, R.J. Spot-welding solid targets for high current cyclotron irradiation. *Appl. Radiat. Isot.* **2016**, *118*, 350–353. [[CrossRef](#)] [[PubMed](#)]
19. Interactions of Ions with Matter (SRIM-2013). Available online: <http://www.srim.org/> (accessed on 5 October 2017).
20. Verel, I.; Visser, G.W.M.; Boellaard, R.; Walsum, S.-V.M.; Snow, G.B.; Van Dongen, G.A.M.S. ^{89}Zr immuno-PET: Comprehensive procedures for the production of ^{89}Zr -labeled monoclonal antibodies. *J. Nucl. Med.* **2003**, *44*, 1271–1281. [[PubMed](#)]
21. Firestone, R.B.; Coral, C.F. *Table of Isotopes*, 8th ed.; John Wiley & Sons: New York, NY, USA, 1999; ISBN 978-0-471-35633-2.
22. Soppera, N.; Dupont, E.; Bossant, M. JANIS Book of Proton-Induced Cross-Sections. *Janis B. proton-induced cross-sections*, ENDF/B-VII.1, TENDL-2011 and EXFOR, OECD NEA Data Bank (OECD NEA Data Bank, 2012). Available online: <https://www.oecd-nea.org/janis/book/book-deuteron.pdf> (accessed on 14 August 2018).
23. Peterson, R.S. Experimental γ ray Spectroscopy and Investigations of Environmental Radioactivity. Available online: <http://citeseerx.ist.psu.edu/viewdoc/download?doi=10.1.1.547.6798&rep=rep1&type=pdf> (accessed on 5 September 2018).
24. Taghilo, M.; Kakavand, T.; Rajabifar, S.; Sarabadani, P. Cyclotron production of ^{89}Zr : A potent radionuclide for positron emission tomography. *Int. J. Phys. Sci.* **2012**, *7*, 2156–2160. [[CrossRef](#)]

